3 November 1998
Version 1.00

TO: Distribution

FROM: Raymond Swartz, MS 168-522, JPL, Ph:818-354-1911

SUBJECT: Metrology Breaks and the SIM Astrometric Grid

1 Introduction

In order to successfully provide high resolution science output, the Space Interferometry Mission requires a well-defined full-sky astrometric grid to provide scale and calibration information. The development of this grid is so critical to the science results that the production of the grid is considered fundamental mission operations. The resulting grid information will be a product provided to the end user.

Starting with the astrometric grid simulation code that Andy Boden described in his memo [2], I have been modifying the code for greater detail and throughput as well as studying the effects of various mission scenarios on the resulting astrometric grid. The main focus of this note is a study of the effects of losing the metrology lock during a grid campaign.

2 The SIM Astrometric Grid

The details of creating and solving for the astrometric grid may be found in Andy's original memo[1], so this note will contain an overview so that this analysis may be understood.

The fundamental measurements that SIM is capable of making is one of the relative delay between two path lengths for the light from an object, calculated by Equation 1, where $\hat{s}$ is the object position vector, $\vec{B}$ is the baseline of the instrument, c is a constant term to deal with object path length differences in the instrument monitored by the internal metrology, and ϵ will be the measurement uncertainty due to finite measurement resolution and systematic uncertainties. For this analysis ϵ was a random gaussian value with $\sigma = 200$pm.

$$d = \hat{s} \cdot \vec{B} + c + \epsilon \tag{1}$$

The baseline of SIM cannot be *a priori* measured to the necessary resolution for microarcsecond position measurements. What we can do is track the relative metrology changes in the baseline from an initial, albeit unknown value. This means that when measuring the separation of two arbitrary objects by measuring their respective delays, the resulting measurement has no directly applicable scale. However, if measurements are made for many interlocking sets of objects covering the entire sky, the knowledge that the whole of the sky covers 4π may be incorporated with those individual measurements to add an angle scale to the measurement. In this way we are able to reconstruct the separation between objects on the celestial sphere, and thus their positions.

Parameter	Distribution
Position (α, δ)	random on sphere, with minimum separation requirement (see text)
Proper Motion (μ)	random direction, gaussian magnitude, 0 ± 0.001 as/year
Parallax (π)	distance is gaussian, 1000 ± 100 parsecs

Table 1: The distributions of the astrometric parameters for the generated grid objects.

Like the baseline length, the attitude of SIM cannot be measured on-the-fly precisely enough in real time. By including the SIM attitude as parameters in the data reduction procedure for science observations, the SIM attitude during a measurement may be determined after-the-fact during data reduction, using any attitude estimates from on-board instruments as an initial estimate.

Although we focused on object positions in the above explanation, the positions of these objects are also modified by their proper motion and parallax when considered at a particular epoch. In a similar manner to the position, these parameters are determined and will contribute in setting a scale for the measurements of science objects.

This important catalog of objects is termed the astrometric grid. The objects shall be selected for their magnitude, stability of motion, and sky location, and will serve as references for other observations. Ideally the grid will consist of objects with no companions and constant magnitude that are uniformly distributed over the entire celestial sphere. The limited astrometric field of view of SIM requires a density of these objects corresponding to about 2000-4000 objects for the 4π celestial sphere.

One final note: in the astrometric calculations presented below, all coordinates are ecliptic coordinates. Since we are working with generated objects, and relative effects of variable instrument conditions, the offsets of real celestial and ecliptic coordinates was an unnecessary complication which contributed nothing to our understanding of the effects observed.

3 Modifications from the Original Code

3.1 The Generated Object Catalog

For these studies, the object catalog generator produced 3000 objects with the characteristics presented in Table 1. During the work that is being presented here, an error was discovered in the program that generated the initial grid objects. In order to maintain whole-sky coverage, in nominal operation a minimum separation between grid objects was imposed. As new objects were generated they were required to satisfy this minimum separation from the previously generated objects before being added to the list. Those that fail this test were rejected, until the desired number of grid objects were generated. In nominal operation the separation in α is normalized by $cos(\delta)$ yielding a parameter we call α_*, but this multiplication was missing in the original generation code. This resulted in more objects than intended being packed into the polar regions, degrading the uniformity of the object density on the simulated celestial sphere.

This bug was discovered and corrected about 70% of the way through this analysis. Expectations were that the effect of this overabundance on the conclusions would be slight, if noticeable at all. By comparing 30 of the grids calculated with the bug with 5 followup grids calculated without the bug (Table 2), no significant difference was seen at the statistical regime of 30 experiments, so we conclude the results of the old and new code could be combined with no effect on the conclusions reached for this paper.

Parameter	Old Generator	New Generator
α_*	2.515 $\pm$ 0.385	2.628 $\pm$ 0.767
δ	2.710 $\pm$ 0.623	2.901 $\pm$ 1.174
μ_{α_*}	4.149 $\pm$ 0.726	4.023 $\pm$ 0.423
μ_δ	4.690 $\pm$ 1.174	4.142 $\pm$ 0.896
π	2.554 $\pm$ 0.226	2.564 $\pm$ 0.253

Table 2: The means and sigmas of the width of the parameter residuals for 30 grids calculated with the old (with the object separation bug) generator versus 5 grids calculated with the new (fixed) generator. All values are in μas. The 10% metrology break probability experiments (explained later in this note) were used for this table, in order to see effects the metrology breaks would have on the distributions.

3.2 Grid Observation Scheduling

The initial model of grid campaigns used a naive linear model for the timing of the grid observations. The total mission time was divided by the total number of grid tiles, and the resulting interval was used between successive tiles. This simple approximation worked just fine for the nominal ideal case, but with the introduction of variable instrument conditions, such as losing metrology lock during a sequence of observations, the timing of the observations becomes more important.

Conceptually, to avoid complications or interruptions in the grid observations it makes sense to scan the entire sky as quickly as possible. This gives little time for changing instrument conditions to develop enough to complicate the grid calculation, and is a model for which one may easily think of an entire-sky survey of grid objects as a "snapshot" of the sky at that epoch. Thus, it is thought that the normal operational mode of SIM should consist, in part, of a series of dedicated grid observation *campaigns*.

Andy Boden has concluded from his studies that an acceptable number for grid observations is 4.5 total-sky grid observation runs per year, and that approximately 20% of the total mission observation time will be spent in the grid campaigns. This time is sufficient for producing the astrometric grid, while allowing time for science observations which use the grid as calibration. The simulation has been modified to model this.

A side effect of the new model of grid observations is that several months elapse between the campaigns. We may conservatively assume that changing instrument conditions during this time will affect the metrology, so it is reasonable that an implicit metrology break be inserted between each grid campaign. This results in the number of baseline metrology lengths being

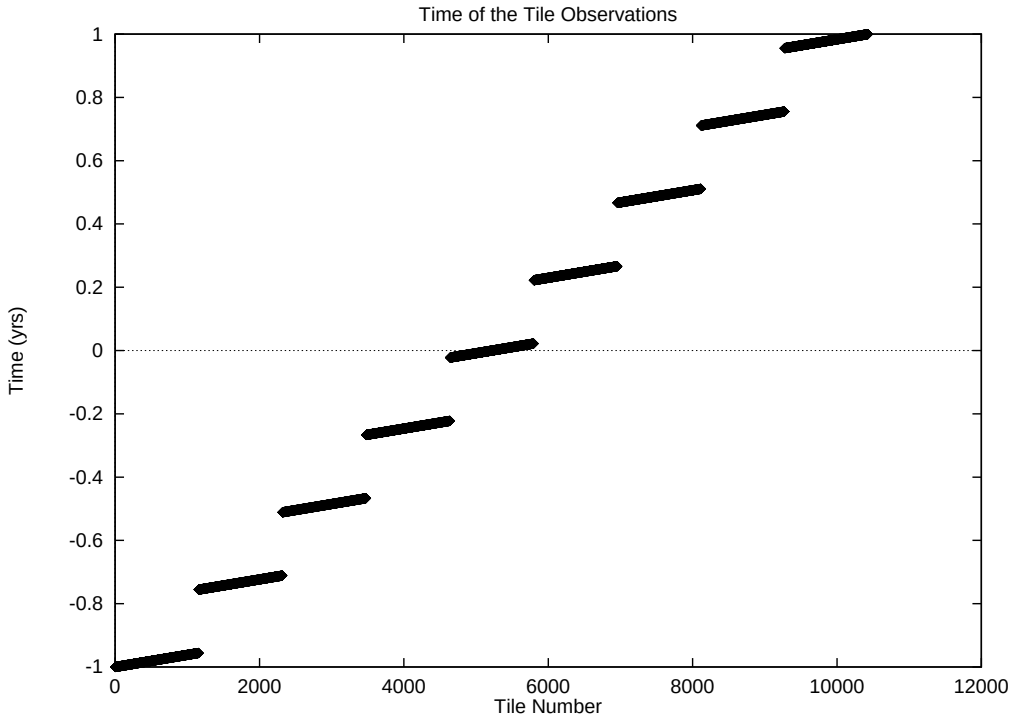

Figure 1: The timing of the grid observation campaigns, using a two-year mission example, as were most of the simulation experiments in this note. Although plotted as discreet points, the individual tile observations for a campaign appear to merge and form a line for that campaign. The intra-campaign gaps are seen as sequence breaks in the vertical direction.

at least equal to the number of grid campaigns. In the analysis below, these implicit metrology breaks are not counted in the metrology break probability that will be used. For example, when reporting a 0% metrology break probability, there is a 0% probability of *additional* metrology breaks beyond the implicit break between campaigns, i.e. no intra-campaign metrology breaks. Thus, a 10% metrology break probability means that for every tile within a grid campaign there is a 10% chance that a metrology break will occur before the simulated tile data is "measured", leading to a metrology break approximately every 10 tiles.

3.3 Conjugate Gradient on Multiple Processors

Mathematically, the problem being solved is essentially the canonical matrix equation shown in Equation 2, for which a two-processor computer (expandable to four) was purchased to calculate the time consuming matrix reductions necessary.

$$\tilde{\mathbf{A}}\vec{\mathbf{x}} = \vec{\mathbf{b}} \qquad \Longrightarrow \qquad (\tilde{\mathbf{A}}^{\mathbf{T}}\tilde{\mathbf{A}})\vec{\mathbf{x}} = (\tilde{\mathbf{A}}^{\mathbf{T}}\vec{\mathbf{b}}) \tag{2}$$

While the original code ran the $A^T A$ calculation using a farm of tens of workstations, the conjugate gradient reduction resulting in the correction vector $\vec{\mathbf{x}}$ used for the next iteration

[1] was written as a sequential calculation, not taking advantage of the multi-processor capabilities. Rewriting the conjugate gradient code for a parallel calculation using the same farm of workstations would cause network communication problems due to the volume of necessary information exchange, so running a parallel version of the CG code on a single multiprocessor machine seemed an ideal solution.

We selected the pthreads[3] library for this task because it is a portable standard and the libraries are available for many machine platforms including Suns and SGIs. Sun and SGI are producing machines with an increasing number of processors, and this trend looks to continue in the future, so taking advantage of the ability to parallelize and port the code early in development is prudent.

3.4 Grid Object Magnitude Effects

The original version of the grid code did not consider the magnitude of the grid objects at all in the simulation. There was no integration time necessary for each observation, and there were no fringe-finding uncertainties due to objects of different magnitude. As of this writing, the code to account for magnitude was inserted into the model, but it was not enabled for this analysis. It will be used for future analysis concerning the quasars for tying the grid to the extra-galactic reference frame.

4 Metrology Breaks

The impetus of this study is the concern that an undetected slow changing of the instrument baseline through the mission might undermine the accuracy of the astrometric grid. Since the astrometric grid is fundamental to the science measurements during the mission, understanding effects such as these is crucial to the success of the mission.

4.1 Modeling a Metrology Break

Seeing the effect of a slow continuous changing of the metrology during a simulated mission is difficult. Small changes in the metrology require corresponding higher statistics to observe resulting effects in the simulation. However, to keep the simulation and grid results realistic, we cannot just arbitrarily increase the number of grid objects that are observed. A realistic grid for SIM consists of 2000-4000 objects (we use 3000 for this analysis) evenly distributed around the entire sky. With this number of objects in the simulation, there are sufficient experiment-to-experiment variations in the width of the grid residuals that we must run many experiments, then use the collected statistics to reach our conclusions.

We model the metrology breaks as a change in the baseline length which, for whatever reason, is not continuously tracked by the external metrology. This gaussian-distributed change (we use $\sigma = 1\mu$m) is applied to the existing baseline so that through the mission the baseline length exhibits a random walk, as seen in Figure 2.

Each new metrology will result in an additional fit parameter in Equation 2 to fit for the new baseline length, which in turn affects how well the section of the celestial sphere measured with that baseline length will fit with the others to form a complete grid.

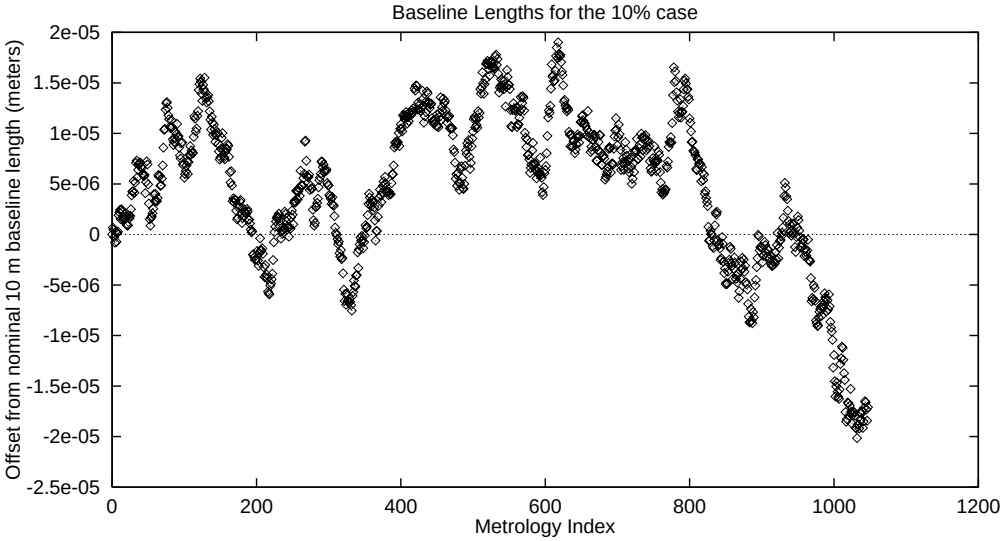

Figure 2: The offset from the nominal 10m baseline length plotted for each metrology break. The gaussian sigma of each length change is 1μm. The case plotted here is one with the metrology break probability set to 10% .

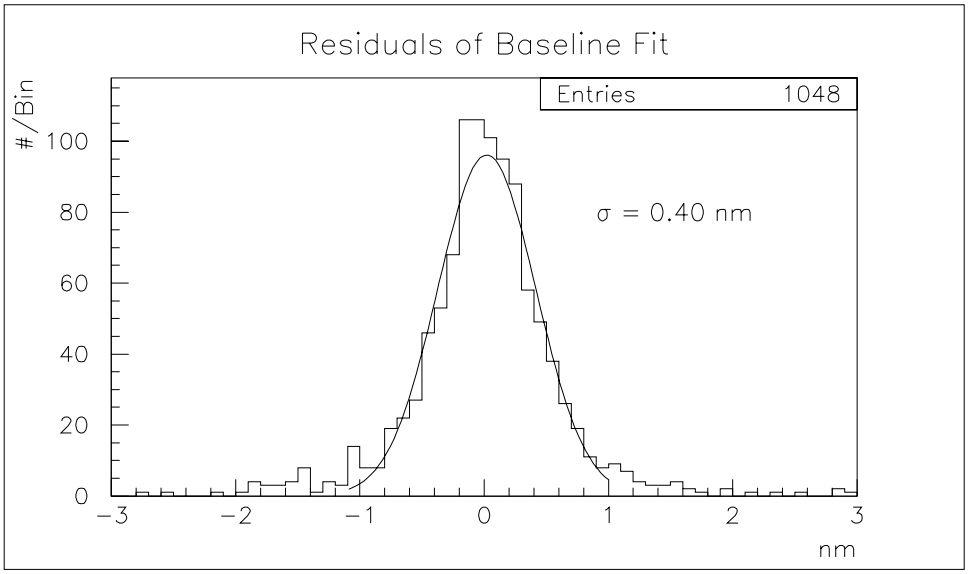

Figure 3: The residuals of the fitted baseline for the experiment shown in Figure 2, with a gaussian fit.

These studies are motivated primarily by the desire to know how accurately the grid can be reconstructed, and the magnitude of uncertainty in reported grid position. Thus we shall report a reconstructed grid result as the spread of the distribution of residuals for the fit parameters. Thus, for the example plotted in Figure 4, the grid is reported to have an α_* resolution calculated as the sigma of the gaussian distribution, which in this case is 1.9 μas for 0% metrology break probability and 3.2 μas for 10% metrology break probability, with similarly calculated results (shown in the Figure) for the other parameters. Statistical arguments will be based on combining the sigma values for the astrometric parameters obtained from multiple runs into a mean performance relative to each metrology break probability.

We note that the distributions of the parameter residuals in Figure 4 show only part of the story. When regions of the celestial sphere are examined separately, as in Figures 5 through 8, we see that the amount of the residuals varies for different regions of the sky. Although the plots for Figure 5 only show position coordinates, this zonal pattern in the residuals is enough to show that there are considerable correlations in the results. The correlations will be examined later in this note.

In this study it is important to remember that we want to see the *relative* effects of increasing the frequency of the metrology breaks. Running the simulation for 5-year experiments takes a lot of time (several days is typical), while much more throughput can be achieved by running 2 year experiments. Relative effects should be similar for the 2 and 5 year cases, so examining relative effects allows an increase in computational efficiency. We shall run a subset of 5 year experiments to act as a sanity check.

5 Results

We compare results by examining the statistical behavior of a number of experiments. We shall combine the resolution values for each experiment with a particular metrology break probability to obtain a mean resolution for that break probability.

5.1 Degradations in the Grid Performance

The simulated 2-year mission results listed in Table 3 show an expected increase as the metrology breaks become more frequent, but (as discussed above) because of the limited mission length and number of observations, the entries in the table are of limited utility. It is more illustrative to examine the *relative* grid performance as we increase the frequency of metrology breaks, allowing us to make direct 2-year and 5-year comparisons to insure that the results are consistent. We do this in Figure 9.

In Figures 9, 10, and 11 we see that the degradation in the grid resolution proceeds slowly for the first few probabilities we tested. Even at the 10% level, the grid resolution still hasn't degraded horribly, increasing the residuals by only 25%. Above 10% the resolution degrades faster, almost doubling the residuals by the time the metrology break probability reaches 25%, and nearly tripling by 50%. Note that the 5 year cases are exhibiting the same behavior, validating our decision to use 2-year missions for these studies.

We had thought that the small degradation in grid performance at the 10% metrology break level was due to observing adjacent tiles between the breaks, resulting in long (on average 10

$P(Break)$	α_*	δ	μ_{α_*}	μ_δ	π
0%(30)	2.124 ± 0.383	2.313 ± 0.701	3.345 ± 0.422	3.547 ± 0.845	1.933 ± 0.112
0.1%(30)	2.216 ± 0.347	2.411 ± 0.719	3.420 ± 0.523	3.818 ± 0.966	1.952 ± 0.102
1%(30)	2.295 ± 0.428	2.574 ± 0.964	3.553 ± 0.605	3.908 ± 1.114	2.029 ± 0.126
10%(30)	2.515 ± 0.385	2.710 ± 0.623	4.149 ± 0.726	4.690 ± 1.174	2.554 ± 0.226
25%(8)	3.496 ± 0.506	4.003 ± 0.981	5.905 ± 1.035	6.861 ± 2.198	3.735 ± 0.366
50%(5)	5.020 ± 0.589	5.854 ± 1.036	10.208 ± 3.954	10.385 ± 5.087	6.087 ± 1.219

Table 3: The distributions of residuals for a set of metrology break probabilities, in μas. The table lists the means and sigmas of the width of the distributions, averaged over the number of experiments shown in the parentheses in the first column. This table demonstrates a degradation in grid precision as the metrology breaks increase in frequency. Note these are from 2 year simulated missions, so these values are not directly indicative of final grid accuracy, but to show the trend as the metrology break probability is increased.

tiles) contiguous regions of the sky being observed for each metrology. We could then expect the grid results would be sensitive to the order the grid tiles were observed. To test this, we ran a few experiments where the order of the grids was completely random, eliminating the contigious regions. No further degradation in the grid was observed, so we consider these results to be robust.

5.2 Correlations in the Grid Solution

Although the iterative conjugate gradient method used for solving Equation 2[1] does not directly yield information on correlations, it is worthwhile to empirically calculate an approximation to the covariance matrix. For example, studies of the wide and narrow angle observations that are currently being conducted need to know the correlated (systematic) and uncorrelated (statistical) uncertainties for the astrometric parameters in order to provide their best results.

We calculate the overall empirical covariance between two fitted astrometric parameters i and j by Equation 3, where r_{ni} is the residual of the fitted value for astrometric parameter i of object n, σ_{ii} is the empirically determined width of the gaussian distribution of residuals for parameter i, and $\langle\rangle$ denotes the expectation (mean) value of the term in the brackets.

$$\rho_{ij} = \frac{\langle (r_i - \langle r_i \rangle)(r_j - \langle r_j \rangle) \rangle}{\sigma_{ii}\sigma_{jj}} = \frac{1}{N\sigma_{ii}\sigma_{jj}} \sum_{n=1}^{N} \sum_{m=1}^{N} (r_{ni} - \langle r_i \rangle)(r_{mj} - \langle r_j \rangle), \qquad n \neq m \qquad (3)$$

Note that we cannot use the simplified form of Equation 3 by replacing the numerator with $\langle (x_i - x_i^T)(x_j - x_j^T) \rangle$, where x_i^T is the true (generated) value of parameter i for the object. This substitution is invalid because, as previously discussed and seen in Figure 4, the means of the residuals for a fitted parameter are not constrained to be zero.

Figure 12 shows a matrix of the plot of these values accumulated globally, so that each object is paired with every other object for purposes of calculating a correlation value, which is then entered into the plots. The figure shows that there are no global correlations.

Of particular interest are the correlations of the astrometric parameters when, instead of summing over the whole sky, a limited region of the sky is sampled. For example, studies of the wide and narrow angle observations that are currently being conducted need to know the correlated (systematic) and uncorrelated (statistical) uncertainties for the astrometric parameters in order to achieve their best results. Such work is performed over a single field-of-regard, and we know from Figure 5 that there are zonal effects in the residuals such that two non-adjacent fields-of-regard may have significantly different correlations. We therefore use the simulation to measure the magnitude of these correlations.

	α	δ	μ_α	μ_δ	π
α	0.711 ± 0.117				
δ	-0.006 ± 0.086	0.699 ± 0.126			
μ_α	0.040 ± 0.258	-0.012 ± 0.098	0.712 ± 0.104		
μ_δ	0.016 ± 0.121	0.032 ± 0.347	-0.016 ± 0.069	0.691 ± 0.121	
π	0.010 ± 0.085	-0.011 ± 0.090	0.032 ± 0.070	0.020 ± 0.083	0.395 ± 0.054

Table 4: Correlations calculated on a single field-of-regard averaged for 30 experiments with the metrology break probability set to 0%. We see significant self correlations for most parameters, except for the low $\pi - \pi$ values. This tells us that for π measurements most of the measurement uncertainty will be local and stochastic in nature.

	α	δ	μ_α	μ_δ	π
α	0.798 ± 0.088				
δ	0.005 ± 0.107	0.783 ± 0.098			
μ_α	-0.056 ± 0.306	0.049 ± 0.204	0.809 ± 0.095		
μ_δ	-0.025 ± 0.192	-0.032 ± 0.398	0.015 ± 0.102	0.806 ± 0.080	
π	0.003 ± 0.134	0.043 ± 0.146	0.023 ± 0.088	0.049 ± 0.192	0.600 ± 0.061

Table 5: Single field-of-regard correlations averaged from 30 experiments with the metrology break probability set to 10%. We note the self-correlation values have increased, indicating the increase of zonal errors, especially for π.

With this in mind we revisit Equation 3 and, instead of summing over all objects in the sky, we sum only for objects within 7.5 degrees (a single field-of-regard radius)) of a "target" grid object. We step through the entire grid so that each object has its turn as the target. The results are listed in Table 5.2, where we see little correlation other than the self-correlations of the parameters. Most of the self correlations are of order 0.7, indicating that most of the uncertainty for those values will be because of zonal effects, as seen in Figure 5. The π self correlation, though, is much smaller. Most of the error in our fitted π results will be of a statistical (random) nature.

This is a pleasing result for distance measurements as random errors tend to cancel out with many observations, so using several of these grid objects as reference points for a science

observation should yield very good distance values for science objects.

We would like to see how these results change as the metrology break probability is increased, so we compare these results with those in Table 5.2, which were calculated using thirty 10% metrology break probability experiments. There is about a 14% increase of the non-π self correlations, indicating an increase of the zonal effects noted above. However the π correlations show a much higher sensitivity, increasing about 50%.

6 Conclusions

The most striking conclusion of this work is that the effects of metrology breaks are not as bad as feared. There were expectations that a metrology break probability of 10% would result in extreme degradation of the astrometric grid due to having too few tiles with a particular metrology to obtain a good metrology fit. While the sensitivity of the π correlations to the 10% case was large, that is still more metrology breaks during a grid campaign than realistically expected, so it should not be the cause of much concern. Overall, the robustness of the grid to small metrology break probabilities is encouraging.

References

[1] A.F. Boden, Memo "SIM Astrometric Grid Simulation Development and Performance Assessment - I" (3 Feb, 1997)

[2] A.F. Boden, personal communication.

[3] B Nichols et al, , "Pthreads Programming", O'Reilly & Associates, Inc., ISBN 1-56592-115-1 (1996)

Distribution:

Andy Boden
Dave Van Buren
Tom Livermore
Mark Colavita
Rudi Danner
Chris Jacobs
Sacha Loiseau
Mark Milman
Jo Pitesky
John Reimer
Stuart Shaklan
Mike Shao
Richard Stoller
Slava Turyshev
Steve Unwin
Dave Van Buren
Jeff Yu

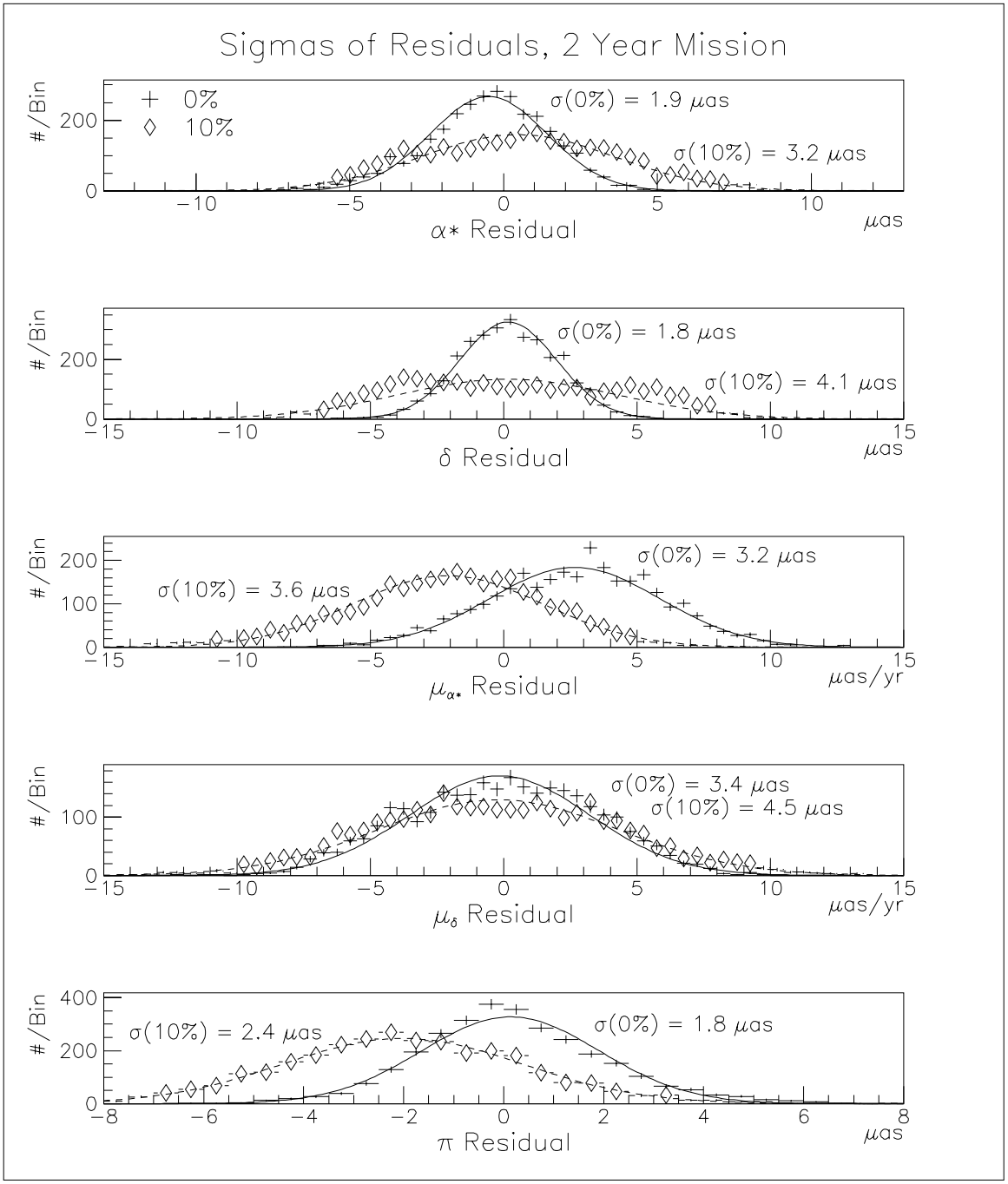

Figure 4: Residuals for grid experiments with 0% and 10% metrology break probability. Note for α directions the plot shows real angles in the α direction, denoted by α_*, and that the matrix reduction is a multi-parameter fit, so there is no requirement that residual for any specific parameter have a mean of zero. The important parameter for this distribution is the σ values of the distributions. We see that the increasing the metrology break probability to 10% increases the width of the distributions, degrading the precision of the grid.

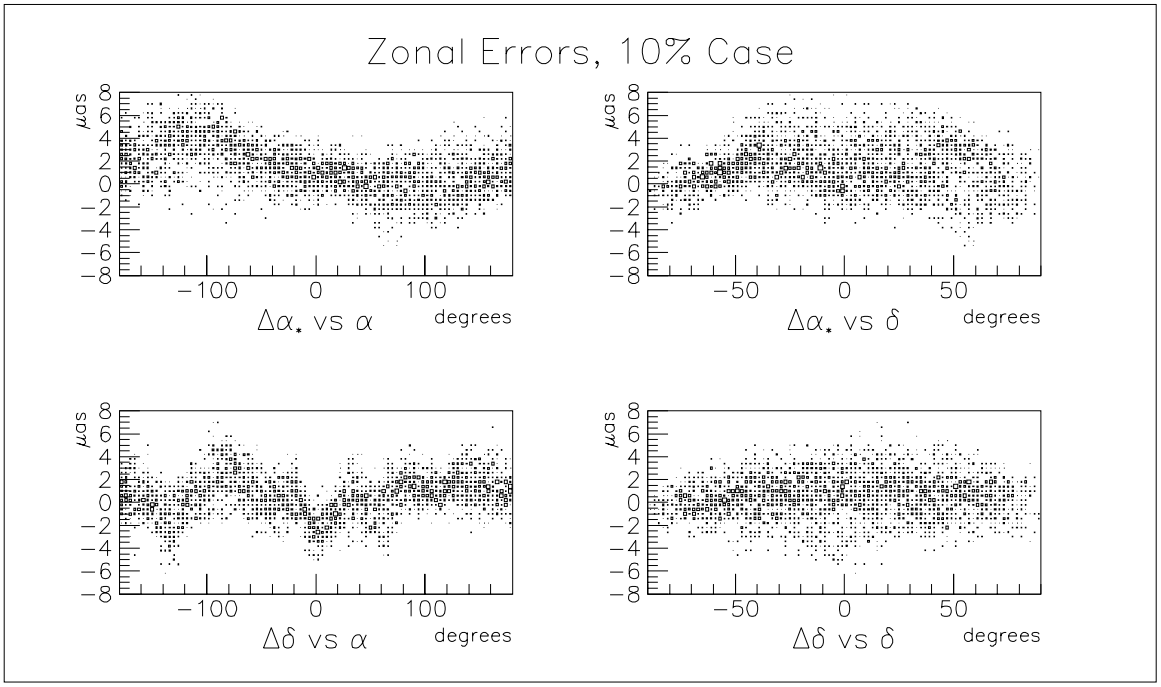

Figure 5: These plots of position residuals versus the position coordinate show significant zonal effects in the residuals. At any point along the horizontal axes of the plots, two types of errors may be discerned by examining a vertical slice: the mean along the vertical axis is the correlated error in the fit for that region, while the vertical spread of the distribution indicates the amount of uncorrelated error at that point. The fact that these values are not constant as one examines the horizontal range of the plot indicates the zonal dependence of the errors.

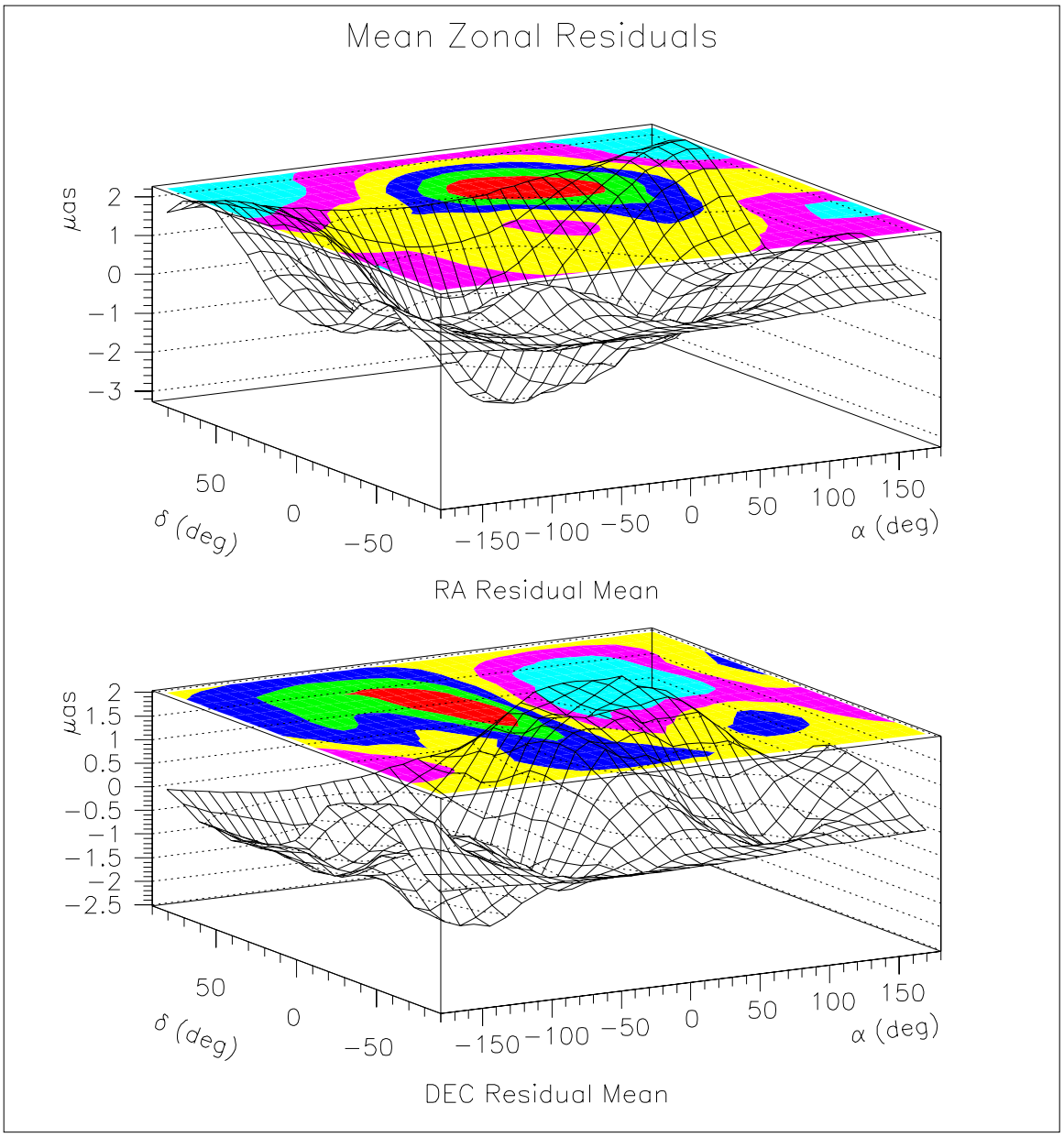

Figure 6: These plots of residuals averaged over a 30 degree radius cone versus the position astrometric parameters show significant zonal effects in the residuals. As in the previous figure, the fact that these values are not constant as one examines the horizontal range of the plot indicates the zonal dependence of the errors.

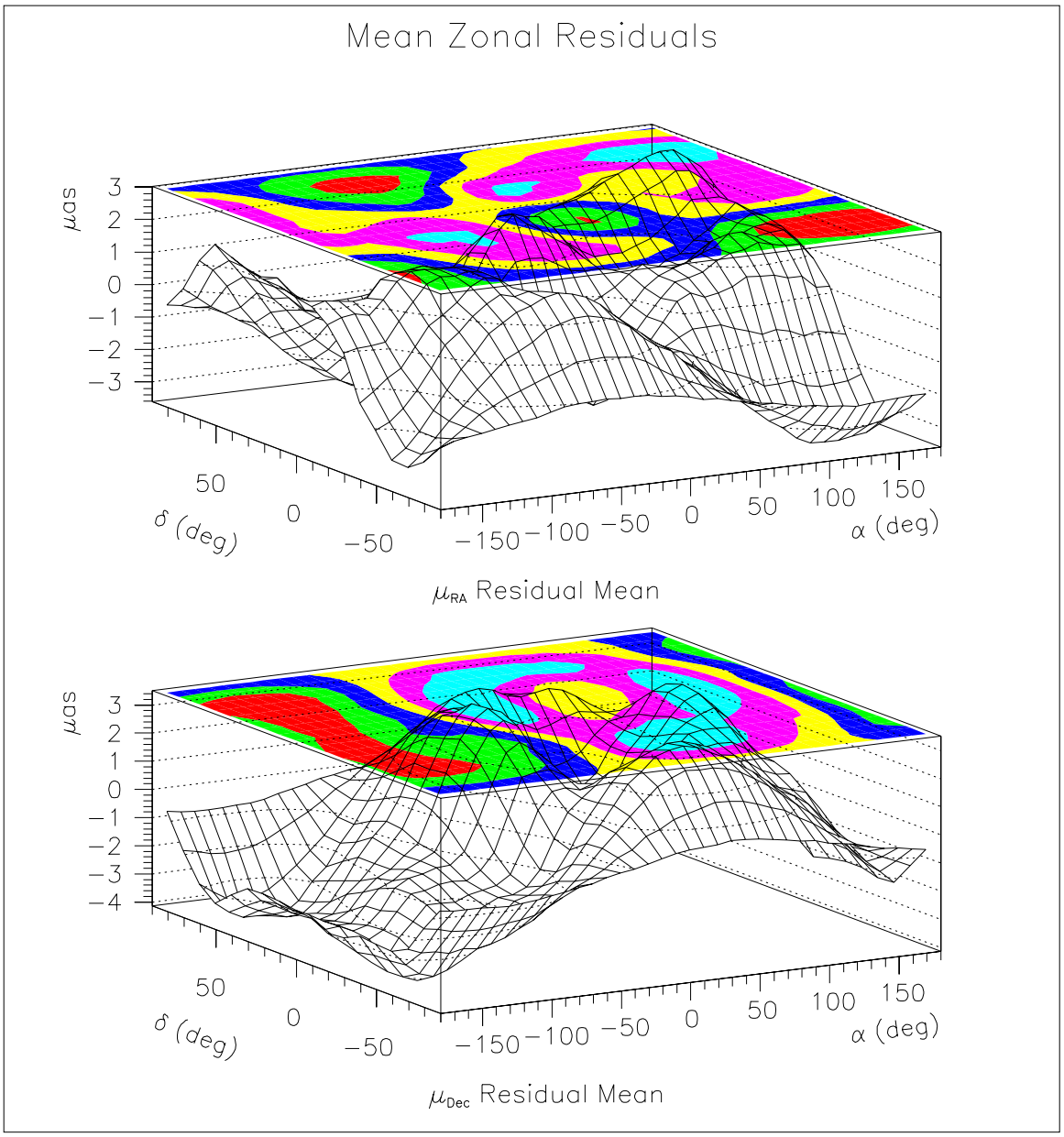

Figure 7: These plots of residuals averaged over a 30 degree radius cone versus the proper mosion astrometric parameters show significant zonal effects in the residuals. As in the previous figure, the fact that these values are not constant as one examines the horizontal range of the plot indicates the zonal dependence of the errors.

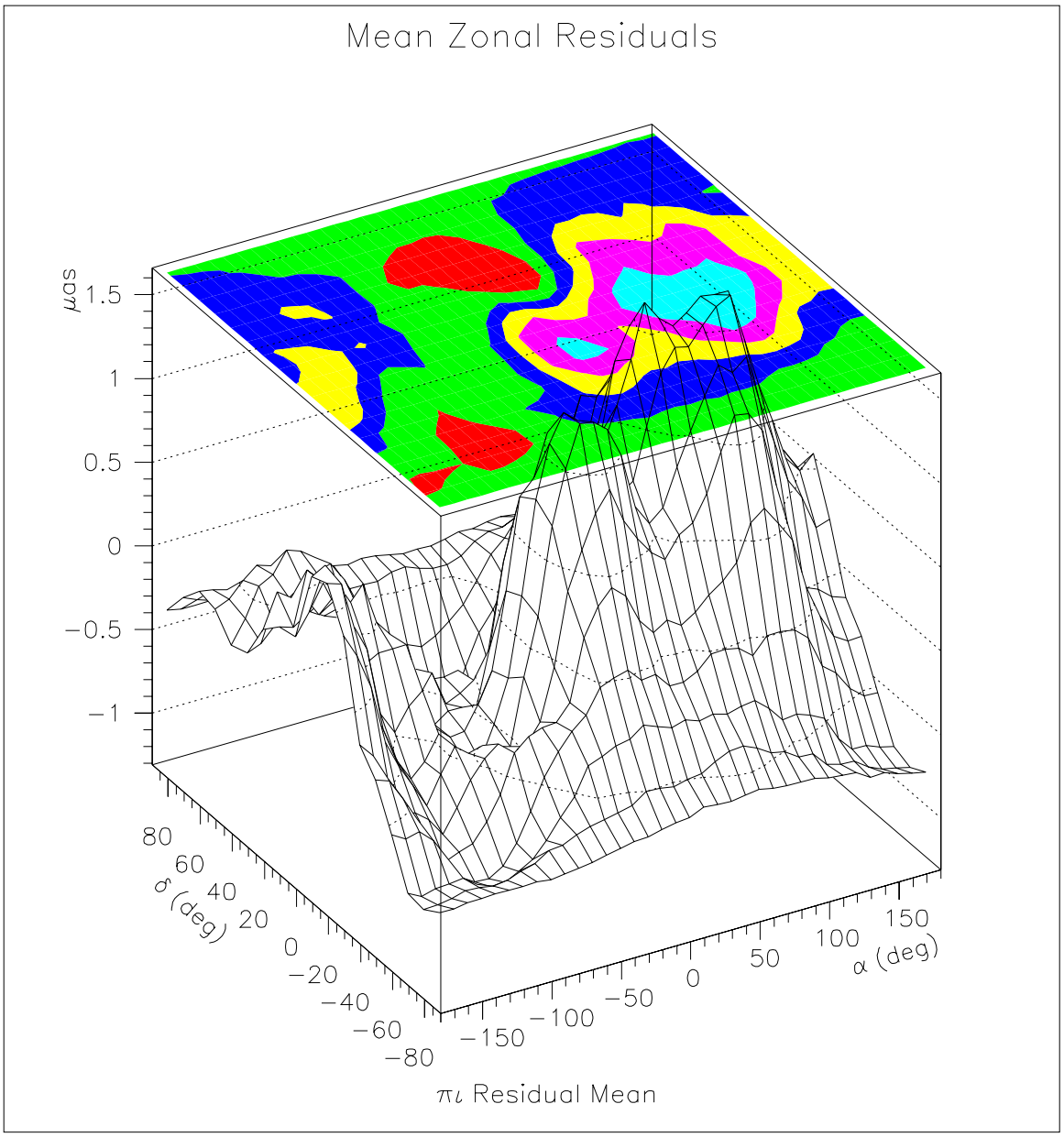

Figure 8: These plots of residuals averaged over a 30 degree radius cone versus the parallax shows significant zonal effects in the residuals. As in the previous figure, the fact that these values are not constant as one examines the horizontal range of the plot indicates the zonal dependence of the errors.

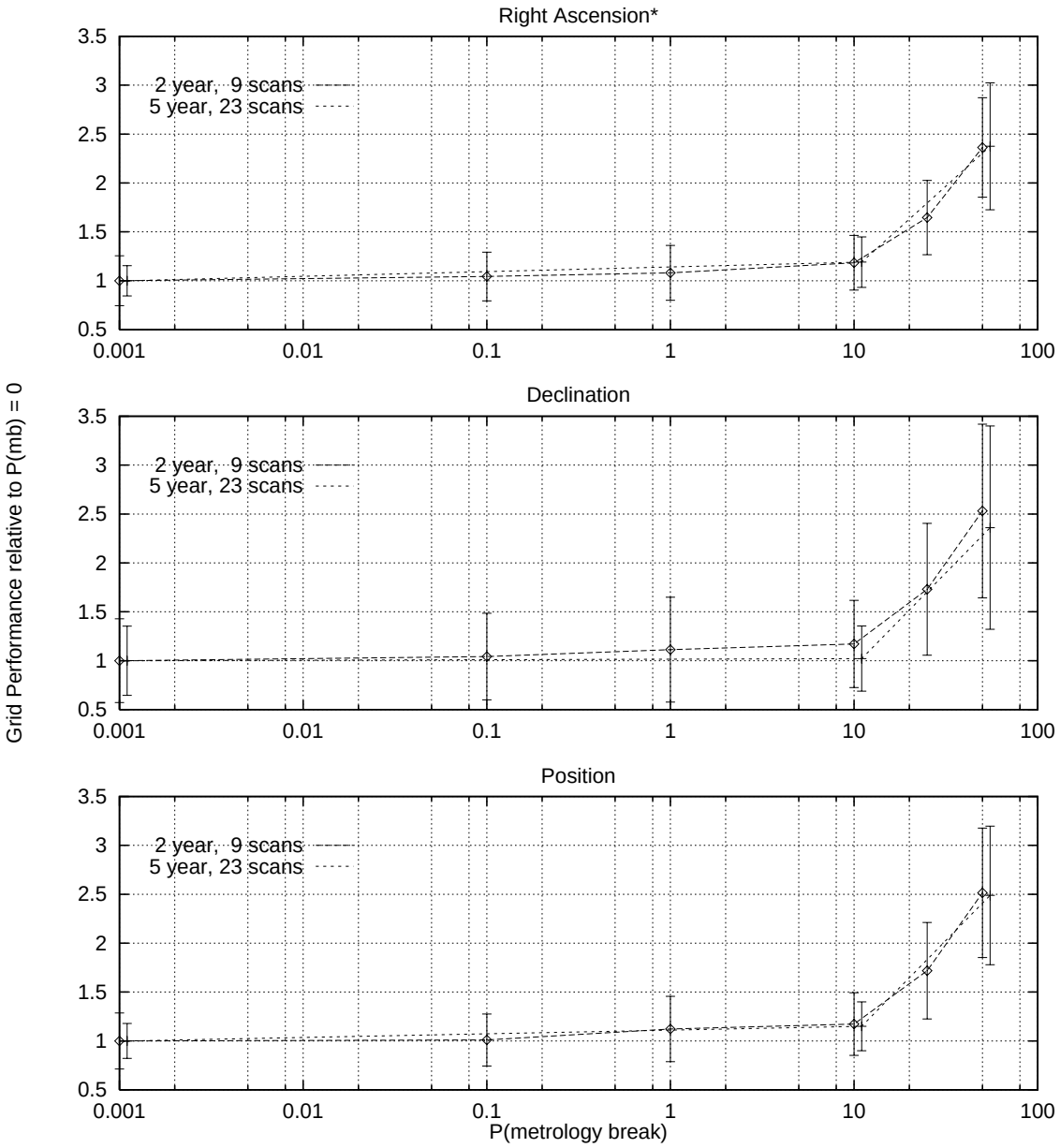

Figure 9: The mean position residuals for various values of the metrology break probability, relative to the residuals for no metrology breaks. The 2 year and 5 year missions are superimposed to demonstrate that the 2 year case sufficiently models the behavior of the 5 year case, justifying the time savings of the 2 year simulation. We also see the combined position result.

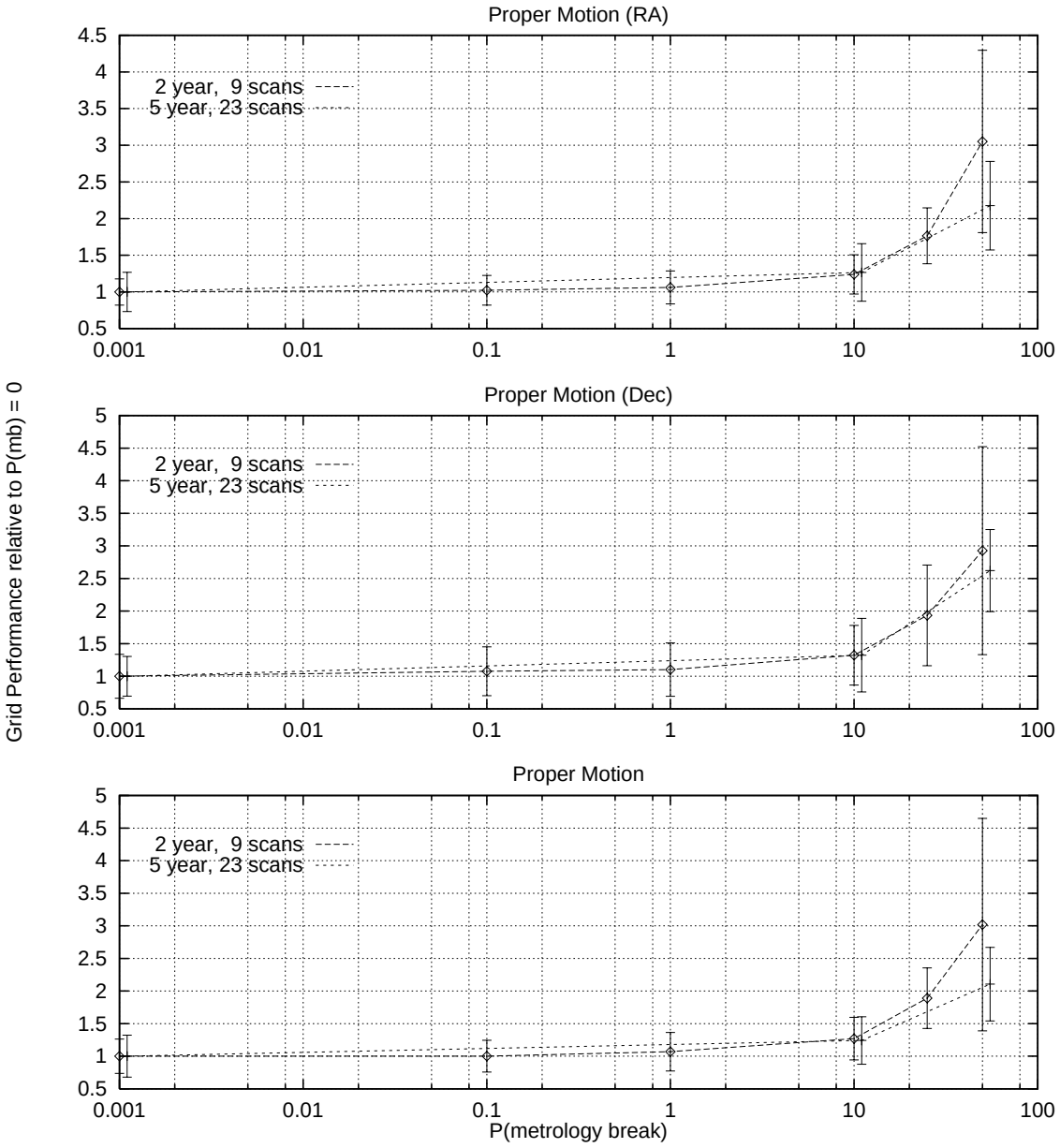

Figure 10: The mean proper motion residuals for various values of the metrology break probability, relative to the residuals for no metrology breaks. The 2 year and 5 year missions are superimposed just as in Figure 9.

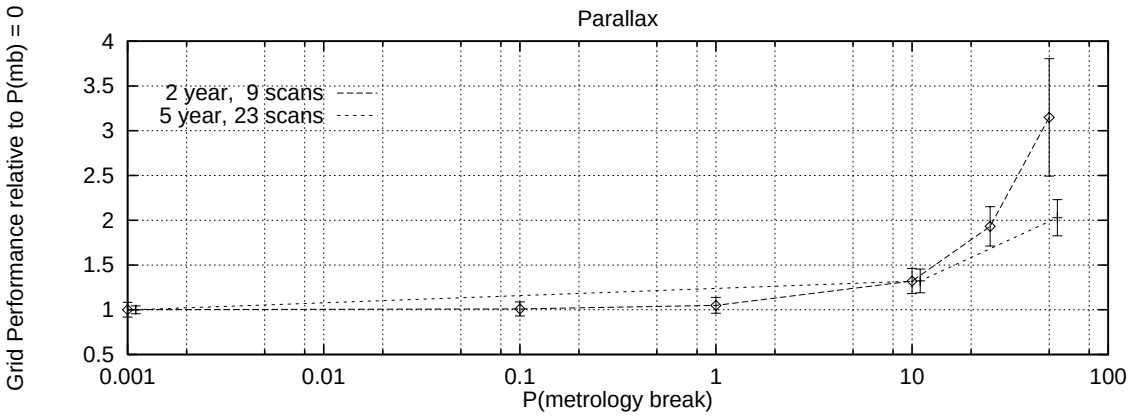

Figure 11: The mean parallax residuals for various values of the metrology break probability, relative to the residuals for no metrology breaks. The 2 year and 5 year missions are superimposed just as in Figure 9. Recall that the higher metrology break probability values were done with a low number of experiments being run, so that the mismatch for the 50% probability is not a cause for concern. This will be verified in the future with more experimental runs for this case.

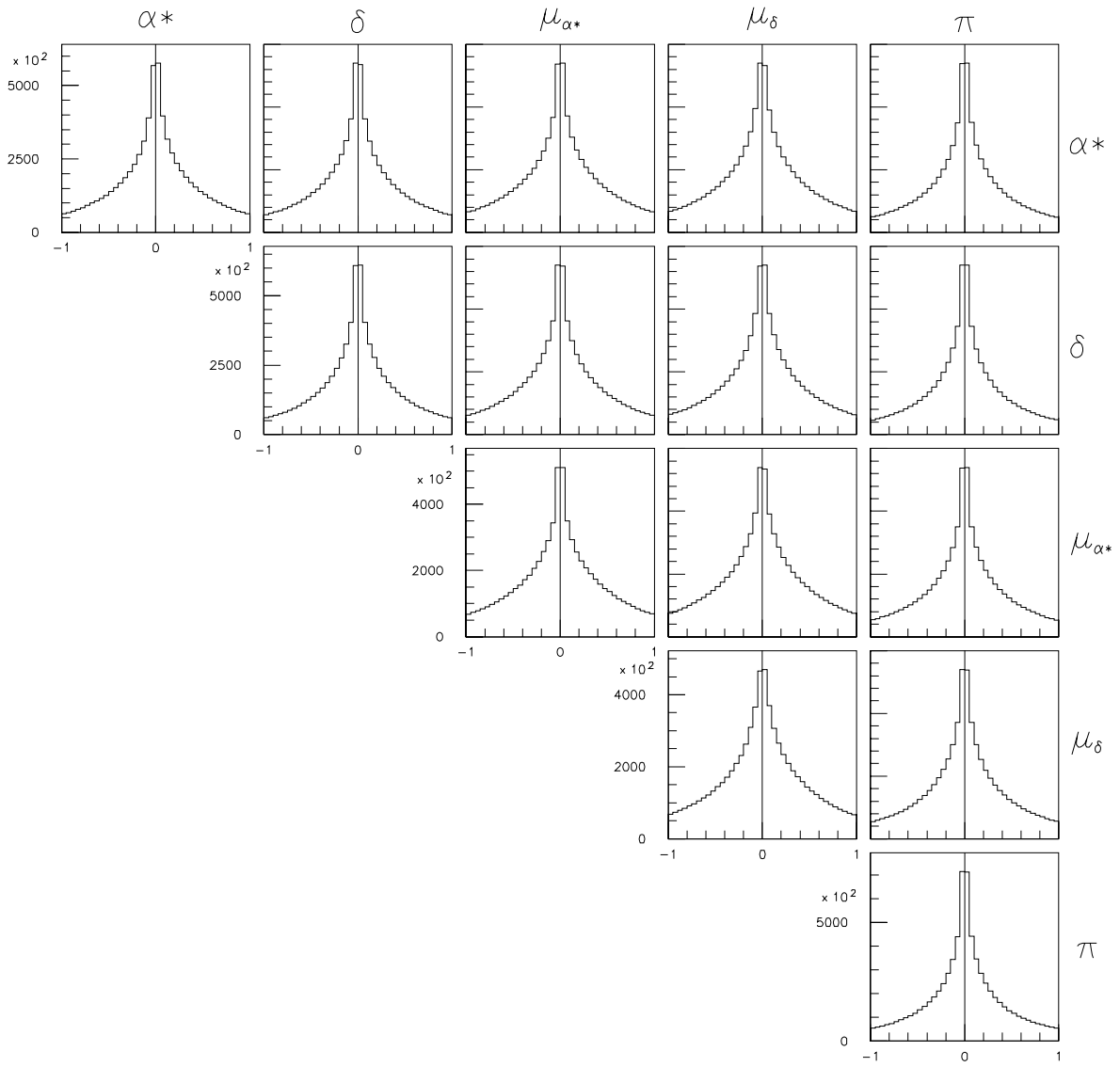

Figure 12: The global correlations between astrometric parameters for a simulated whole-sky grid, calculated using Equation 3, where each pair of objects has a single entry on each histogram. Note that when the entire grid is considered, the local correlations seen in Figure 5 do not correspond to global correlations. Also, as this is an empirical calculation, it is possible for the entries in these histograms to be > 1.

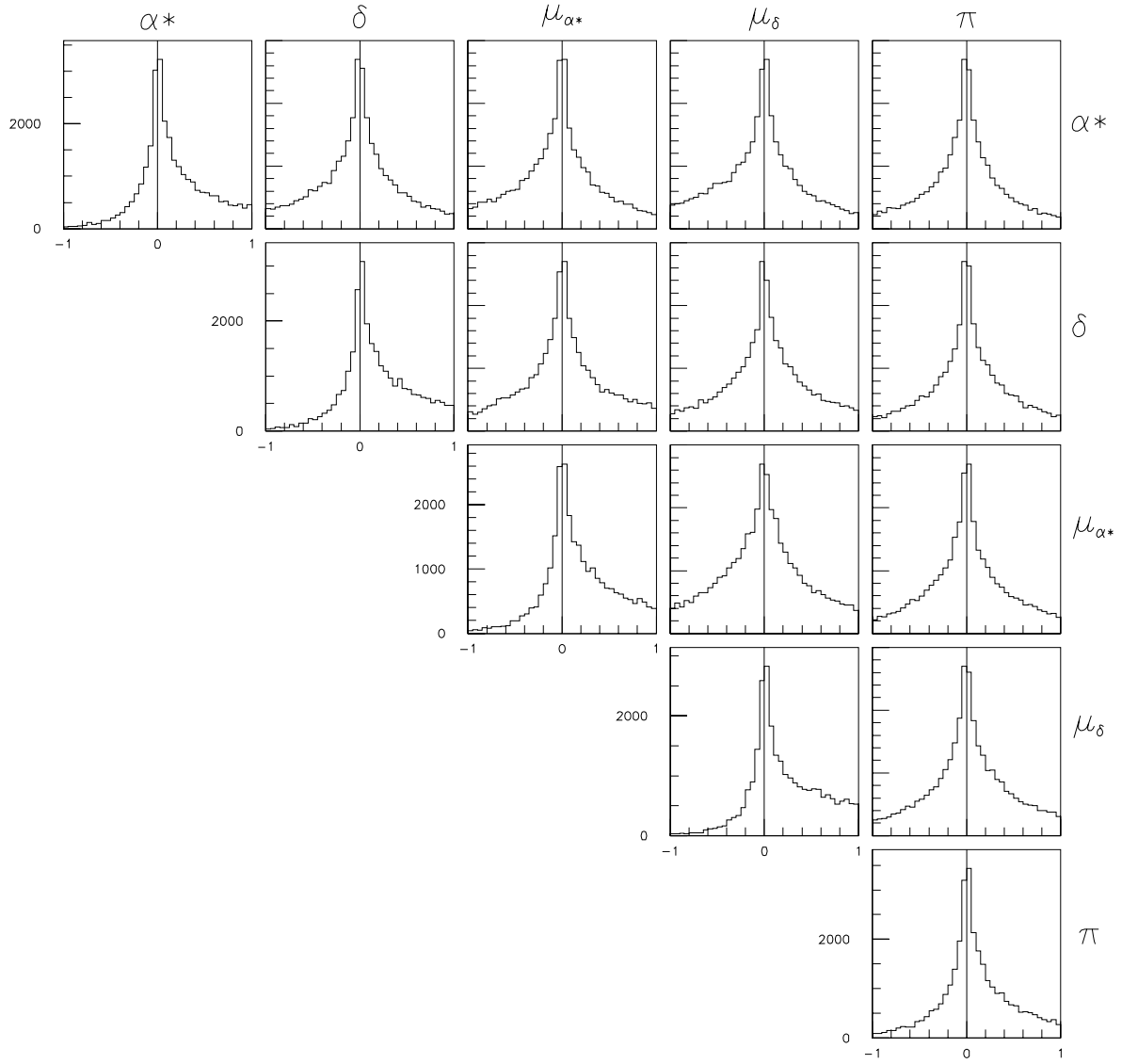

Figure 13: The local correlations between astrometric parameters for a sample simulated whole-sky grid, again calculated using Equation 3. In this case, objects are paired with others that are within a single field-of-regard angular radius (7.5 degrees). The correlations appear as asymmetries in the plots, and are especially pronounced on the diagonal. This is caused by the same zonal errors seen in Figure 5. The metrology break probability for this sample is 0%.